Int. J. Electrochem. Sci., 8 **(2013)** 9785 - 9800

International Journal of
ELECTROCHEMICAL
SCIENCE
www.electrochemsci.org

Study of the Role of Boric Acid During the Electrochemical Deposition of Ni in a Sulfamate Bath

C.E. Dávalos, J.R. López, H. Ruiz, Alia Méndez, R. Antaño-López, G. Trejo[*]

Laboratory of Composite Materials and Functional Coatings. Center for Research and Technological Development in Electrochemistry (CIDETEQ). Parque Tecnológico Sanfandila, Pedro Escobedo, A.P. 064, C.P. 76703, Querétaro, México.
[*]E-mail: gtrejo@cideteq.mx

Received: 16 April 2013 / *Accepted:* 30 May 2013 / *Published:* 1 July 2013

Electrodeposition of nickel from a sulfamate bath with and without boric acid was studied using linear voltammetry, electrochemical impedance spectroscopy (EIS) and electrochemical quartz crystal microbalance (EQCM) techniques. In the absence of boric acid, nickel hydroxide was formed in the potential range from -0.6 to -1.4 V due to an increase in the pH value close to the electrode surface caused by hydrogen evolution. On the other hand, in the presence of boric acid, in the potential range from -0.9 to -1.3 V the results suggest nickel deposition and the reduction of the boric acid. The formation of nickel hydroxide and metallic nickel, in the absence and presence of boric acid, respectively, was confirmed by AFM.

Keywords: Boric acid, EQCM, Electrodeposition, Nickel

1. INTRODUCTION

Nickel coatings were among the first commercially electrodeposited thin metallic films [1,2]. The first nickel bath was formulated by Watts in 1916 [3], and this bath is still used today because of its simplicity and low cost.

Nickel coatings obtained through electrodeposition are commonly used at an industrial level. They provide protection against corrosion and wear resistance through a relatively economical process. The properties of these coatings, such as hardness, corrosion, and wear resistance, are determined by their morphology, microstructure, content of metallic impurities, grain size and porosity [4], features that depend on the composition of the electrolyte bath [5], the current density [6], pH [7,8], temperature [9,10] and additives [11,12].

Nowadays, several different electrolytic solutions are used for nickel deposition, including sulphate [5,13], chloride [8] and sulfamate electrolytes [14].

In the Watts and chloride electrolytes, the Ni electrodeposition conditions differ in their buffer composition, the electrodeposition potential, etc. [11]. In chloride electrolytes, the activity of Ni^{2+} ions is higher and metal deposition potential is lower compared to sulfate electrolytes. Electrodeposits obtained in chloride electrolytes with high chlorine concentrations shave different texture and higher internal stress [15] than those obtained in Watts electrolytes.

The mechanism of Ni^{2+} reduction from acid sulfate solution has been extensively studied by Wiart et al. [16-18] using Watts electrolytes. It is generally acknowledged that the electrocrystallization of the Ni^{2+} ion occurs in several steps, and two successive faradaic reactions have been suggested. The first one involves the formation of Ni^{+}_{ads} ions, and the second one corresponds to a subsequent reduction to Ni. However, in the presence of freshly deposited nickel, H^+ is reduced to H_{ads}, which strongly bonds to the electrode surface and inhibits further reduction of the metal [5].

Moreover, pure Ni deposits plated from nickel sulfamate bath generally exhibit lower internal stress than those from sulfate or chloride baths [19].

Boric acid is one of the main compounds in electrolytic baths for nickel deposition. Some authors state that boric acid is added to the electroplating bath as a buffering agent [8]. Because the pK_{a1} value of boric acid is 9.14, its predominant form in acidic media up to pH 5 is as an undissociated molecule. This indicates the absence of any buffering action of boric acid in these baths. It seems that the influence of boric acid on Ni electrodeposition is complicated [20] and still remains unclear.

In this regard, studies conducted by EI-Shafei and Aramata [21] using cyclic voltammetry have shown that boric acid adsorbs on the Pt (111) surface. Also, Vicenzo and Cavallotti found that this species has a clear influence on the crystallographic structure: its addition to the sulfate electrolyte at pH above 4 extends the stability field of the [100] texture and improves its quality [22]. Mayanna et al. [23] using cyclic voltammetry, showed evidence that boric acid is reduced to diborane when Ni is deposited from a Watts bath. On the other hand, with results obtained using Electrochemical Quartz Crystal Microbalance (EQCM), Song et al. [13] proved that the presence of the boric acid in a sulfate bath enhanced the under potential deposition (UPD) of nickel on Pt. In similar studies, Supicová et al. [24] found that, in the presence of high concentration of boric acid, there is an inhibition of nickel deposition and improved morphology, brightness, and adhesion of the deposited Ni.

The aim of this work was to study the role of the boric acid during the Ni electrodeposition process on a Pt substrate from a sulfamate electrolyte. Electrochemical studies were carried out by linear voltammetry, electrochemical impedance spectroscopy (EIS) and Electrochemical Quartz Crystal Microbalance (EQCM) techniques. Atomic force microscopy (AFM) was employed to study the morphology of the deposits.

2. EXPERIMENTAL

The study of nickel deposition was performed using solutions S_0 (= 400 g L^{-1} $Ni(NH_2SO_3)_2$) and S_0 with 30 g L^{-1} H_3BO_3. These solutions were prepared immediately prior to each experiment using deionized water (18 MΩ cm) and analytical grade reagents of the highest purity available (Sigma-Aldrich). Before each electrochemical experiment, the solutions were deoxygenated for 30 min with ultra-pure nitrogen (Praxair), and the experiments were carried out under a nitrogen atmosphere at 25.0 ± 0.5 °C.

The electrochemical and microgravimetric study was carried out in a conventional three-electrode cell with a water jacket. A quartz crystal microbalance (Maxtek, Mod. 710) and a potentiostat/galvanostat (Autolab, Mod. PGSTAT 30) controlled by independent computers, were used simultaneously to measure the frequency of the quartz crystal and electrochemical parameters. An AT-cut quartz crystal of nominal frequency f_0 = 5 MHz, covered on both sides with Pt film (Maxtek, CA), was used as the working electrode (Pt-QCM). The geometric area of the Pt-QCM electrode was 1.37 cm^2. The real area of the electrode was estimated to be 4.70 cm^2 from the charge corresponding to desorption of a H_{ads} monolayer on polycrystalline platinum (0.210 mC cm^{-2}) [25]. An $Hg/HgSO_4$ electrode and a graphite rod were used as the reference and counter electrodes, respectively. All reported potentials are referred to $Hg/HgSO_4$ electrode. In order to minimize iR-drop effects, the reference-electrode and working-electrode compartments were connected with a Luggin capillary.

The QCM signal was recorded as Δf (= f-f_{initial}) as a function of the electrode potential. The experimental frequency change can be expressed as:

$$\Delta f = -C_f \Delta m + \Delta f_\eta + \Delta f_r + \ldots \qquad \text{(Eq. 1)}$$

Where the first term on the right-hand side of Eq. (1) is the Sauerbrey term [26], which represents the total mass change at the electrode surface. Other possible contributions to the frequency change include changes in the solution viscosity (Δf_η) [27] and the surface roughness (Δf_r) [28,29]. Experimental studies have shown that surface roughness can drastically affect the resonance frequency. This effect was attributed to rougher surfaces having a higher quantity of solvent molecules trapped in surface cavities [30]. In the present work, the use of polished Pt-QCM electrodes (roughness 1.2 nm, as measured by AFM) should have minimized the effects of surface roughness, and the effects of viscosity variations were expected to be negligible. Prior to the measurements, the sensitivity factor (C_f = 0.030 Hz ng^{-1}) of the quartz crystal was determined using the chronoamperometry calibration method described by Vatankhah et al. [31].

Electrochemical impedance measurements were carried out from 100 KHz to 10 mHz, amplitude of 10 mV, using a PARSTAT 2273 potentiostat. Each experiment was started when equilibrium was reached after immersing the working electrode in the solution for two hours.

Atomic force microscope (AFM) (Asylum Research, Mod. MFP-3D) was used in tapping mode to image the deposited nickel on the steel substrate. These measurements were performed in air (ex-situ) using silicon nitride AFM tips (Asylum Research). All images were obtained at 2 Hz and are represented in the so-called height mode, in which the highest portions appear brighter.

3. RESULTS AND DISCUSSION

3.1 Study of Ni electrodeposition in the absence of boric acid

3.1.1 Linear Voltammetry and EQCM Studies

The electrodeposition of nickel onto Pt was studied using a base solution (S_0 = 400 g L^{-1} $Ni(NH_2SO_3)_2$. Initially, simultaneous linear voltammetry and EQCM study were conducted. The potential scan was started from the open circuit potential (E_{OCP}) in the negative direction, over the potential range -0.20 to -1.4 V.

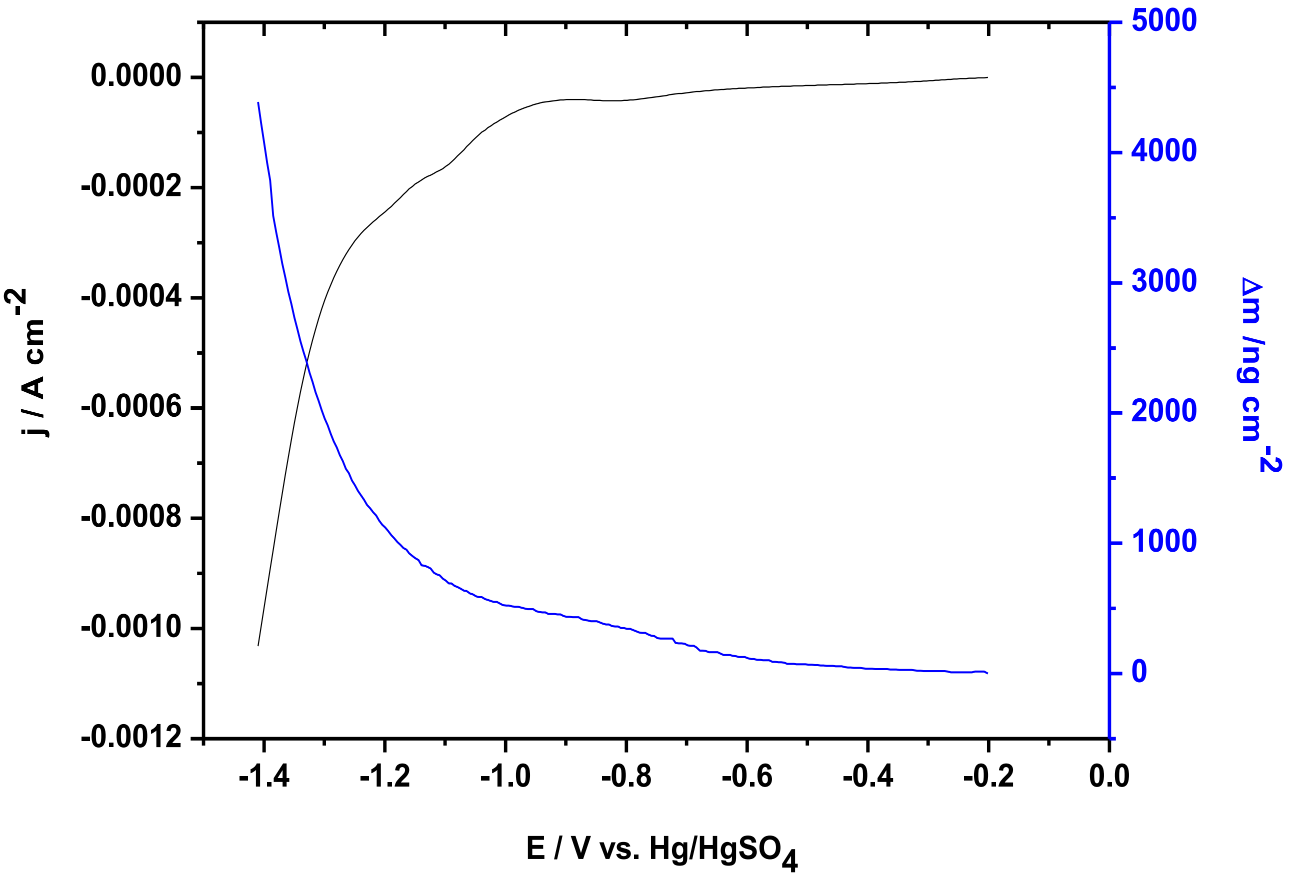

Figure 1. (a) Linear voltammogram and (b) Δm *vs.* E plot for a Pt-EQCM electrode in solution S_0 (=400 g L^{-1} $Ni(NH_2SO_3)_2$) , v = 50 mV s^{-1}.

Fig. 1 shows a typical linear voltammogram recorded for Ni deposition onto Pt from the S_0 solution. It presents a slightly increasing current at -0.6 V followed by a significant increase in current at potentials beyond -0.95 V. Finally, at potentials more negative than -1.25 V the cathodic current increases abruptly. This behavior is similar to that reported by Song [13], where a significant current starts at -0.60 V vs. SCE, due to favorable hydrogen evolution reaction (HER) kinetics at the platinum surface during the cathodic direction scan in the $NiSO_4$ solution. Fig. 1 also shows the change in mass on the electrode surface as a function of potential simultaneously measured by EQCM during the recording of the linear scan voltammetry. During the initial cathodic scan, in the potential range from -0.3 to -1.0 V, a constant increase in the electrode mass was observed. Subsequently, the mass on the electrode increased abruptly at -1.2 V.

A convenient method for making a detailed quantitative identification of the adsorbed species was suggested by Uchida et al. [32-34], who used Faraday´s Law to analyze the anions adsorption on Au:

$$\Delta m = \Delta Q * M/nF \qquad \text{(Eq. 2)}$$

Where Δm corresponds to mass changes per unit area, ΔQ is charge density, M is molar mass, n is the number of electrons transferred, and F corresponds to the Faraday constant. Thus, equation 2 provides a linear relationship of Δm versus ΔQ with a single slope equal to M/nF that allows calculating the molar mass of the adsorbing species. Fig. 2 shows the plot of charge vs. mass obtained from Fig. 1. Charge was calculated from the linear voltammogram by integrating the current with respect to time.

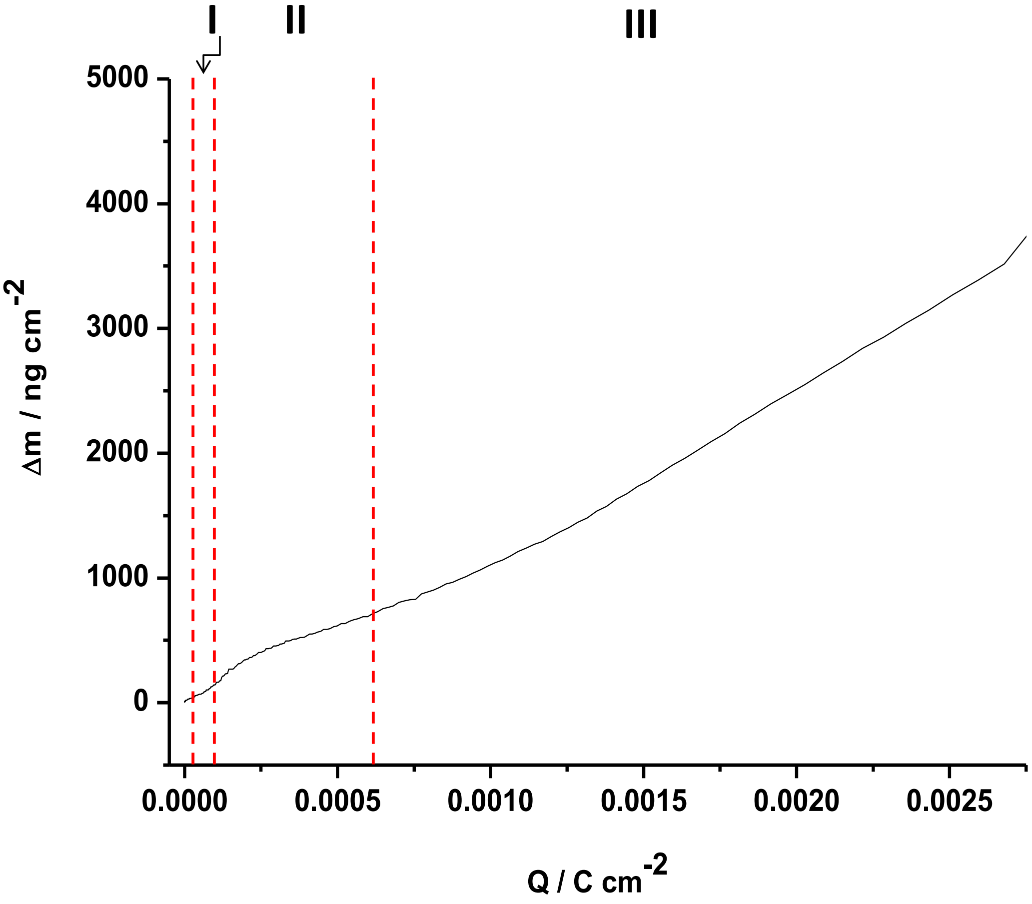

Figure 2. Absolute values of Δm versus Q obtained from Fig. 1

In figure 2, three regions (designated I, II, III) with different linear slopes are delimited. Slope values were then transformed by Faraday´s law, into molar masses (PM/n) (table I). PM/n values obtained in the three linear regions are almost four times greater than the theoretical value of 25 g/mol expected for Ni electrodeposition. This suggests the formation of both UPD Ni [35] and $Ni(OH)_{2(s)}$ on the electrode surface for region I, and Ni + $Ni(OH)_{2(s)}$ for the regions II and III. $Ni(OH)_{2(s)}$ would be formed if the interfacial pH at the cathode surface rises sufficiently to allow this process [8].

The increasing current at about -1.2 V is due to both deposition of pure nickel on Pt and hydrogen evolution, which take place at potentials very close to each other. As a result of these two reactions, the platinum electrode in the unstirred solution is now coated with nickel and the solution is locally more alkaline. Consequently, nickel ions in the interfacial region precipitate as $Ni(OH)_{2(s)}$ on the electrode.

Table1. PM/n values obtained from Fig. 2

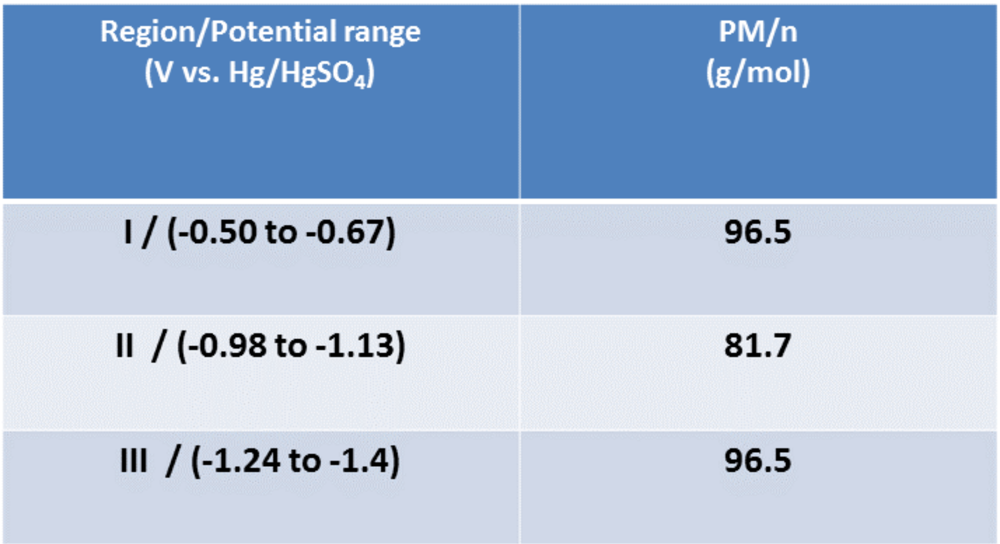

Region/Potential range (V vs. $Hg/HgSO_4$)	PM/n (g/mol)
I / (-0.50 to -0.67)	96.5
II / (-0.98 to -1.13)	81.7
III / (-1.24 to -1.4)	96.5

3.1.2 Electrochemical Impedance Spectroscopy Measurements

Figure 3 shows the impedance spectrums obtained with S_0 (= 400 g L^{-1} $Ni(NH_2SO_3)_2$ in the potential range from -0.90 to -1.42 V vs. $Hg/HgSO_4$. All the spectrums have a capacitive loop at high frequencies, which is related to the double layer charge distribution coupled to the charge transfer resistance.

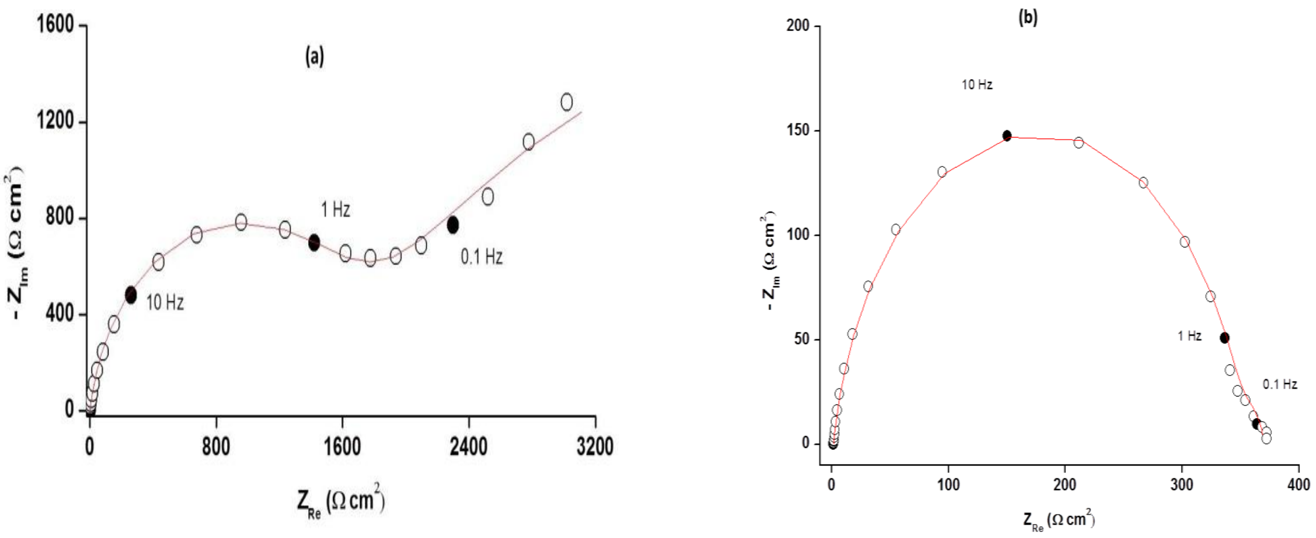

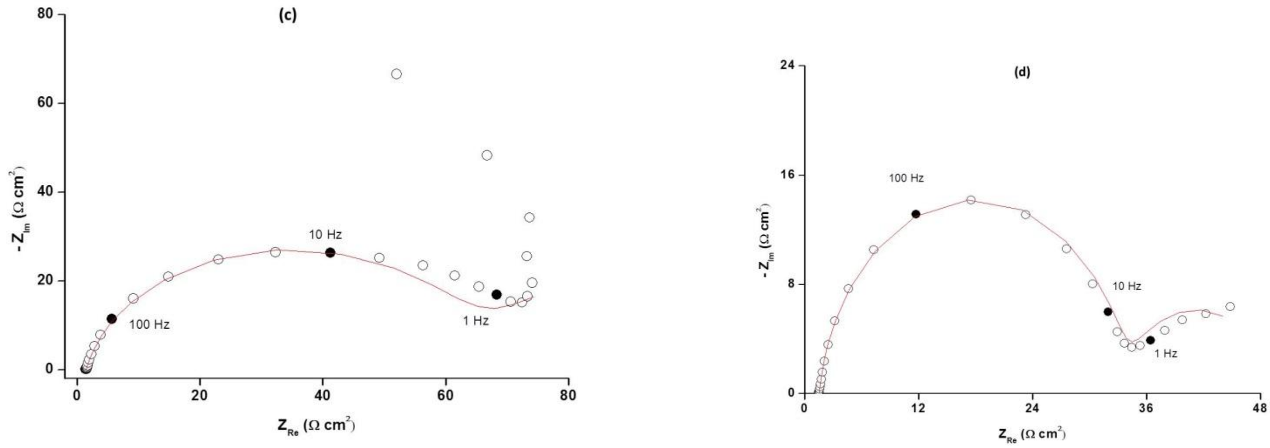

Figure 3. Complex plane impedance spectra for the electrolyte containing 400 g L^{-1} $Ni(NH_2SO_3)_2$, obtained at different potentials: a) -0.90 , b) -1.14 , c) -1.24, d) -1.42 V *vs*. $Hg/HgSO_4$. The circles indicate the experimental data and the solid line represents the fitting curve.

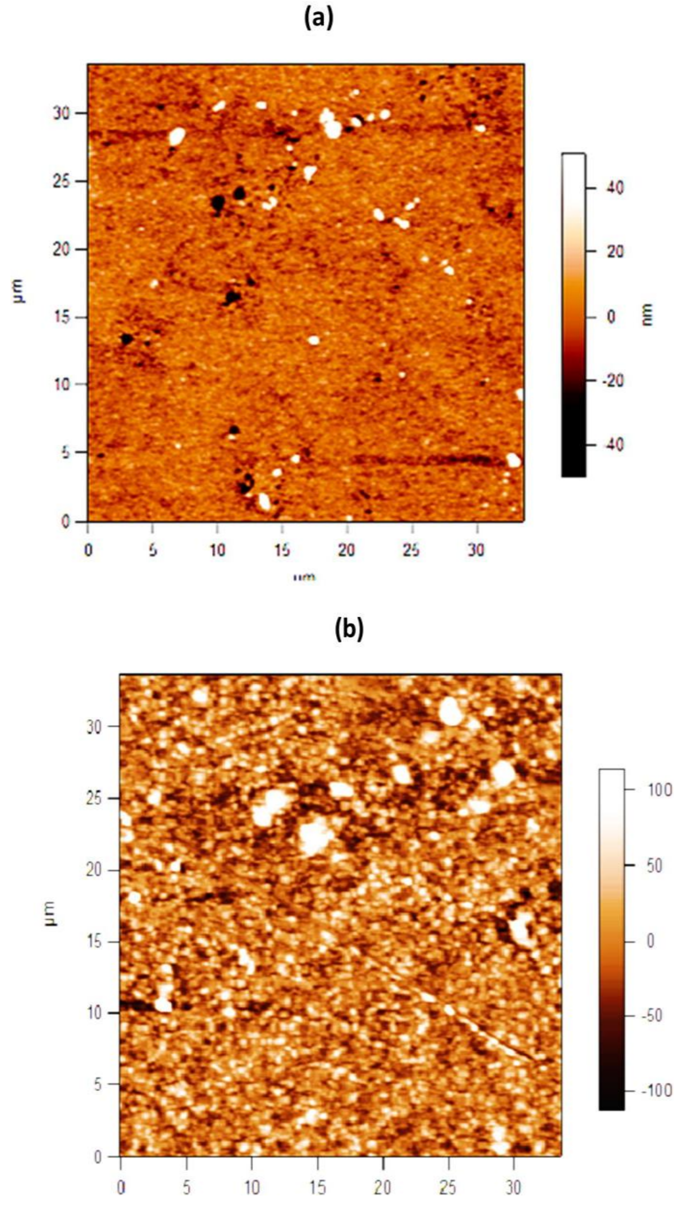

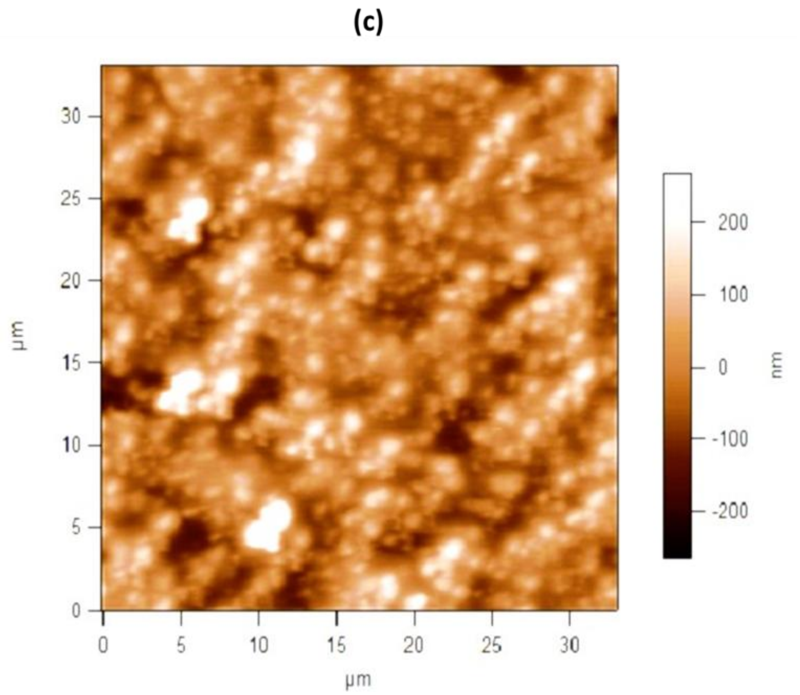

Figure 4. AFM images of nickel electrodeposition onto Pt-QCM electrode at: a) -1.0 V, b) -1.25 V and c) -1.4 V vs. Hg/$HgSO_4$. t = 15 min, Solution S_0 (=400 g L^{-1} $Ni(NH_2SO_3)_2$).

At -0.90 V (fig. 3a) a fragment of a large capacitive loop can be seen in the low frequency domain. This second loop can be associated with adsorption related to H^+ reduction, since this is the prevailing reaction in this potential range. With increasing cathodic polarization (-1.14 V), this capacitive loop tends to decrease (Fig. 3b), indicating that this reaction is enhanced. Thus, its contribution to total impedance is smaller.

At -1.24 V (Fig. 3c) this low frequency loop disappears, but another loop going counterclockwise into the negative region of real part appears. This behavior is typical of systems where a passivation layer is being developed on the electrode [36]. Thus, this feature supports the assumption that $Ni(OH)_{2(s)}$ is precipitating on the electrode surface.

At more cathodic potentials (-1.42 V, Fig. 3d) this reversed loop is replaced by another capacitive loop, which could be indicative of a more complex process involving re-dissolution of the passive layer.

Figure 4a shows the AFM image obtained when the potential scan was held at $E_{Deposition}$ = -1.0 V for 15 min in S_0 solution. This image shows a substrate completely covered by a porous coating due to hydrogen evolution under these conditions.

A nickel deposit was obtained by holding the potential ($E_{Deposition}$) at -1.25 V for 15 min. An AFM image of this surface (Fig. 4b) shows an amorphous deposit. Similar behavior was obtained when the deposition was carried out at $E_{Deposition}$ = -1.40 V, t = 15 min in S_0 solutions. In addition, the size of the clusters increased significantly (Fig. 4c).

These results confirm that the insoluble species $Ni(OH)_{2(s)}$ is formed on the electrode surface due to the hydrogen evolution and the resulting increase in the interfacial pH.

3.2 Ni electrodeposition in the presence of boric acid

3.2.1 Linear Voltammetry and EQCM Study

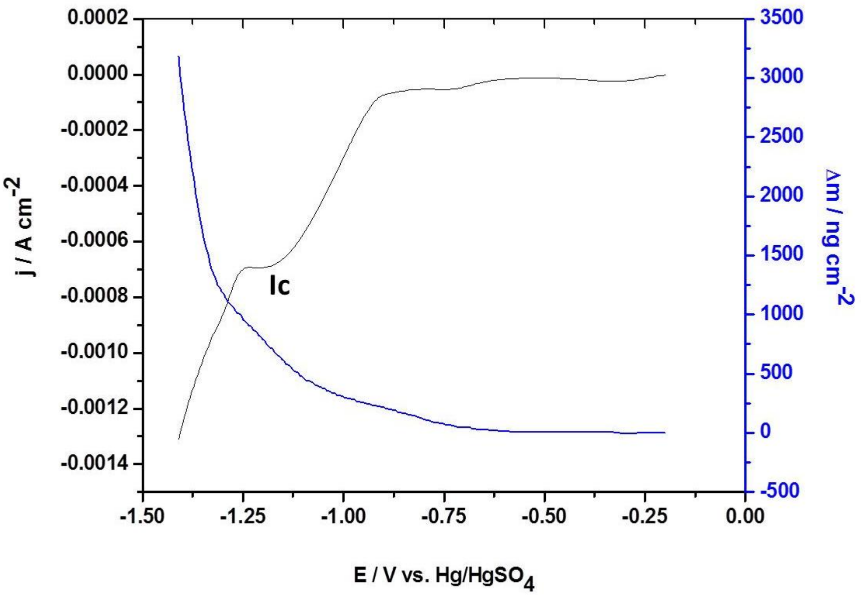

Figure 5. (a) Linear voltammogram and (b) Δm *vs.* E plot for a Pt-EQCM electrode in solution S_0 (=400 g L^{-1} $Ni(NH_2SO_3)_2$) with 30 g L^{-1} H_3BO_3), v = 50 mV s^{-1}.

Fig. 5 shows the linear voltammogram obtained for nickel electrodeposition from S_0 (= 400 g L^{-1} $Ni(NH_2SO_3)_2$) solution with 30 g L^{-1} H_3BO_3. An increase in the cathodic current from -0.88 V up to -1.125 V is observed, followed by a slight decrease at potentials near -1.25 V, and finally a significant increase at potentials beyond -1.25 V is present. This behavior is similar to that reported by Song et al. [13] during the reduction of nickel in $NiSO_4$ solution.

Comparing voltammograms obtained in S_0 solutions without (Fig. 1) and with (Fig. 5) boric acid, it can be observed that in both cases the current increases abruptly at a similar potential value (~-1.25 V), which corresponds to the nickel electrodeposition and hydrogen evolution reactions.

Fig. 5 also shows the change in mass on the electrode surface as a function of potential (Δm *vs.* E), obtained simultaneously to the linear voltammetry. Un like graph without boric acid (Fig. 1), the Δm vs. E plot in presence of this species shows several slope changes as a function of potential: the mass on the electrode surface increases slightly during the cathodic scan in the potential range from -0.7 V to -1.0 V. At more cathodic potentials, in the range from -1.10 to -1.30 V, an increase in the slope is observed. This behavior indicates that the overall adsorption process on the electrode surface is changing. Finally, from -1.3 V to -1.4 V, a new change in the adsorption process is occurring.

Following the data treatment method proposed by Uchida et al. [32,33] to determine which species would most probably be adsorbed on the electrode surface during a potential scan, the Δm vs. Q curve (Fig. 6) was constructed from the plots of Fig. 5. The linear relationships obtained displayed three distinct slopes: region I, region II and region III. The slope values were then transformed, by Faraday´s law, into molar masses (PM/n) (table 2).

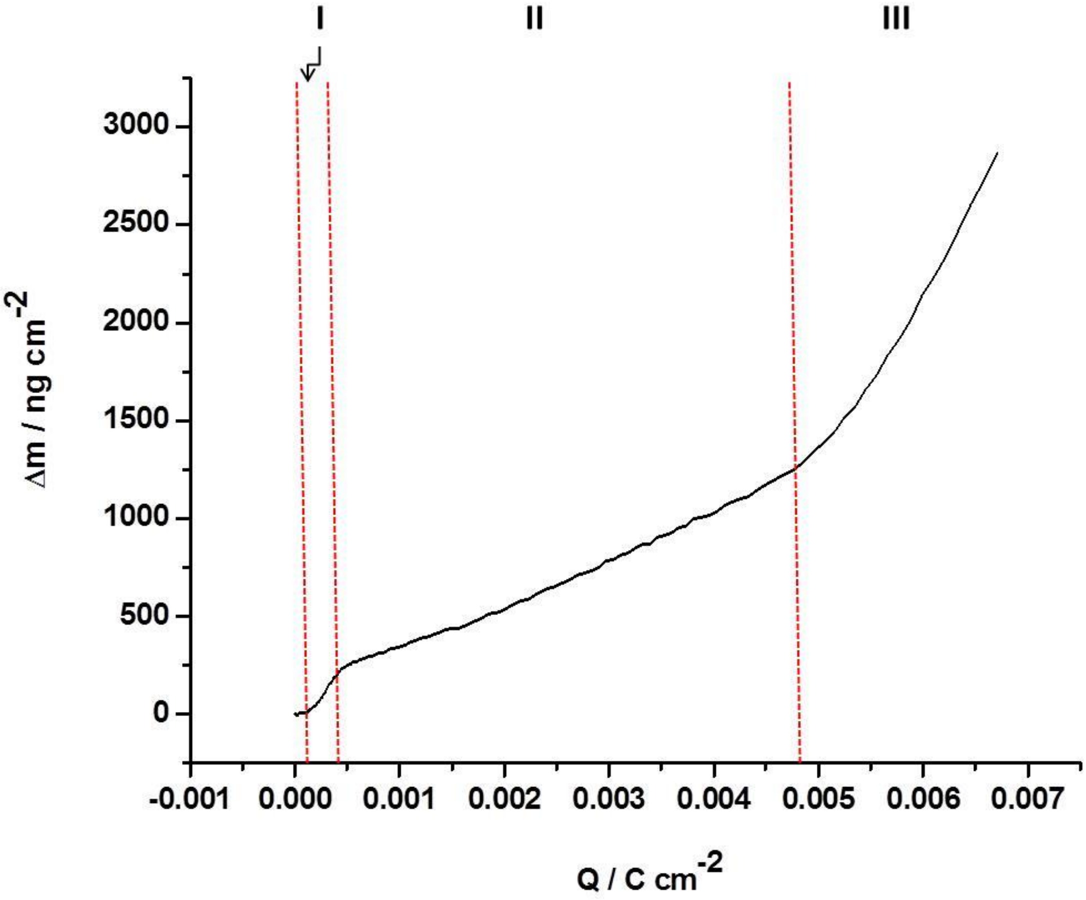

Figure 6. Absolute values of Δm versus Q obtained from Fig. 5.

Table 2. PM/n values obtained from Fig. 6

Region /Potential range (V vs. Hg/$HgSO_4$)	PM/n (g/mol)
I / (-0.70, -0.91)	**77.1**
II / (-0.95, -1.30)	**24.0**
III / (-1.33, -1.40)	**93.7**

In region I, the calculated value of the ratio PM/n was 77.1 g mol^{-1}, wich is three times the theoretical value (25 g mol^{-1}) expected for nickel electrodeposition. This result suggests, as mentioned above, the formation of both: UPD Ni and $Ni(OH)_{2(s)}$ species on the electrode surface, which would occur if the pH at the cathode surface rises sufficiently to allow the production of hydroxide.

In region II, the ratio PM/n was 24.0 g mol^{-1}, which is smaller than the theoretical value for Ni electrodeposition (25 g mol^{-1}), indicating that a fraction of the total charge involved during Ni electrodeposition might be consumed to reduce other minor species. In the voltammogram presented in Fig. 5, the formation of a reduction peak (peak Ic) at the same potential interval can be observed. Thus, it is likely that the reduction of boric acid to diborane occurs at this potential range (equation 3) [23].

$$2H_3BO_3 + 12H^+ + 12e^- \rightarrow B_2H_6 + 6H_2O \qquad \text{(Eq. 3)}$$

Therefore, the current increase in this potential range is due to the deposition of nickel on platinum and the reduction of boric acid.

In region III, the value of PM/n obtained (93.7 g mol^{-1}) is almost four times greater than the theoretical value (25 g mol^{-1}) for Ni electrodeposition. This behavior is similar to that obtained during the nickel electrodeposition in the absence of boric acid, at the same potential interval (*section 3.1.1*). Therefore, the larger mass increase per unit charge, as compared to that for Ni electrodeposition, suggests the formation of both Ni and $Ni(OH)_2$ on the electrode surface.

3.2.2 Electrochemical Impedance Spectroscopy Measurements

Figure 7 shows the Nyquist spectrums obtained for different potentials during nickel reduction in S_0 solution in presence of boric acid. For all of the impedance spectra, the formation of a capacitive loop at high frequencies, associated with the double layer capacitance coupled to the charge transfer resistance is observed. At E = -1.0 V and -1.25 V, the diagrams shows a large capacitive loop in the low frequency domain (Figs. 7a and 7b). This behavior can also be related to the reduction of H^+ ions to gaseous hydrogen, that becomes the main reaction at this potential range [37].

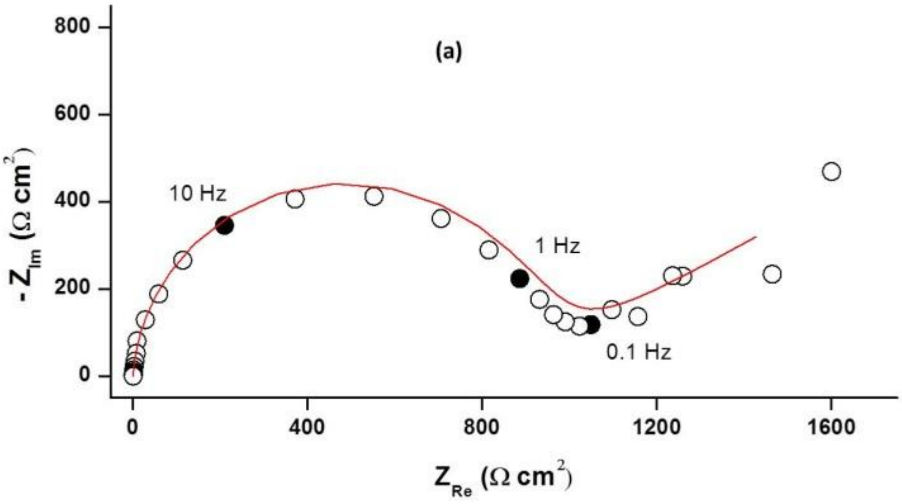

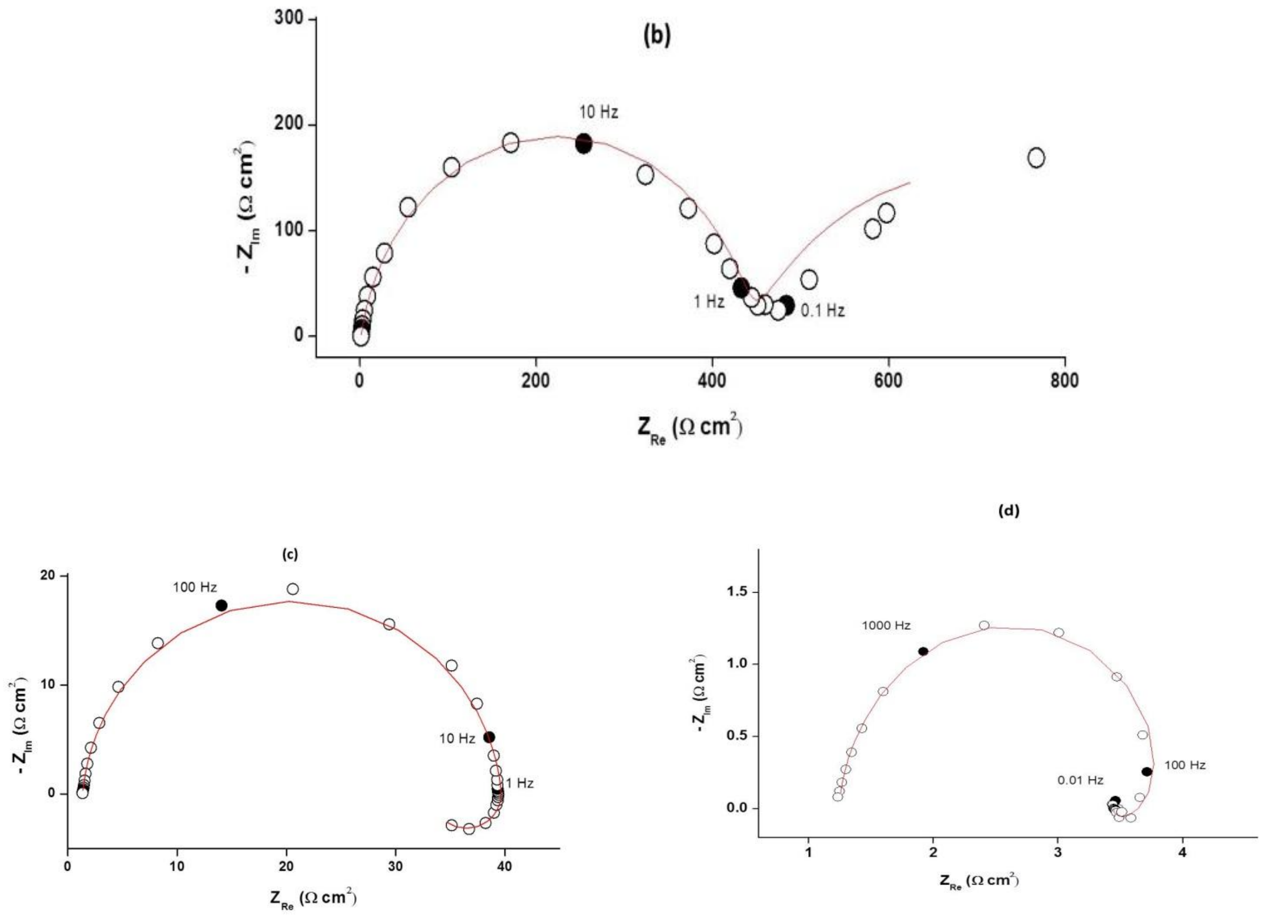

Figure 7. Complex plane impedance spectra for the electrolyte containing 400 g L^{-1} $Ni(NH_2SO_3)_2$ with 30 g L^{-1} H_3BO_3, obtained at different potentials: a) -1.10 V, b) -1.25 V, c) -1.30 V, d) -1.40 V *vs*. $Hg/HgSO_4$. The circles indicate the experimental data and the solid line represents the fitting curve.

When the spectra were obtained at more cathodic potentials (-1.30 V), the capacitive loop tends to disappear and an inductive loop arises at 1Hz of frequency (Fig. 7c). At this potential, nickel electrodeposition begins with high efficiency. Consequently, it is assumed that the inductive loop is generated by the adsorption of a reaction intermediate in the nickel reduction.

Furthermore, the small capacitive loop at low frequency (0.01 Hz) can be related to the H_{ads}^{+} intermediate (Fig. 7d), according to Mattos et al. [38].

The impedance spectrum obtained in the absence and in the presence of boric acid can be suitably fitted using the equivalent circuits shown in Fig. 8. Although many elements can be used for modeling of the impedance spectra, those presented in Fig. 8 were selected as most realistic. In each case, it is indicated the potential range in which the corresponding circuit was used. Circuit equivalent parameters were obtained by using Zview software, and table III summarizes the more important parameters. For experiments performed at -1.1 V and -1.24 V, the charge transfer resistance values (R_{tc}) when the boric acid is not present in Ni dissolution are slightly higher. At -1.30 V the charge transfer resistance is one order of magnitude higher than that in the presence of H_3BO_3. It is important to note that this behavior is present in the range where the adsorption and/or reduction stages of Ni are predominant, indicating that the increase in the values of the charge transfer resistance can be due to the formation of a passivation layer ($Ni(OH)_{2(s)}$), enhanced in absence of boric acid.

Also, the values for the double layer capacitance (C_{dl}) are higher when the boric acid is not present. These results are in agreement with Holm and O'Keefe [10], who suggest that under non ideal conditions the formation of a $Ni(OH)_2$ layer inhibits or interferes the Ni reduction, decreasing substantially the quality of the Ni coatings obtained. Thus, the presence in the impedance spectrum of a capacitive loop with a high capacitance value is associated with poor coating features [10]. Therefore, considering that the higher the surface porosity, the higher the superficial area, and consequently a higher capacitance, the above discussion is consistent.

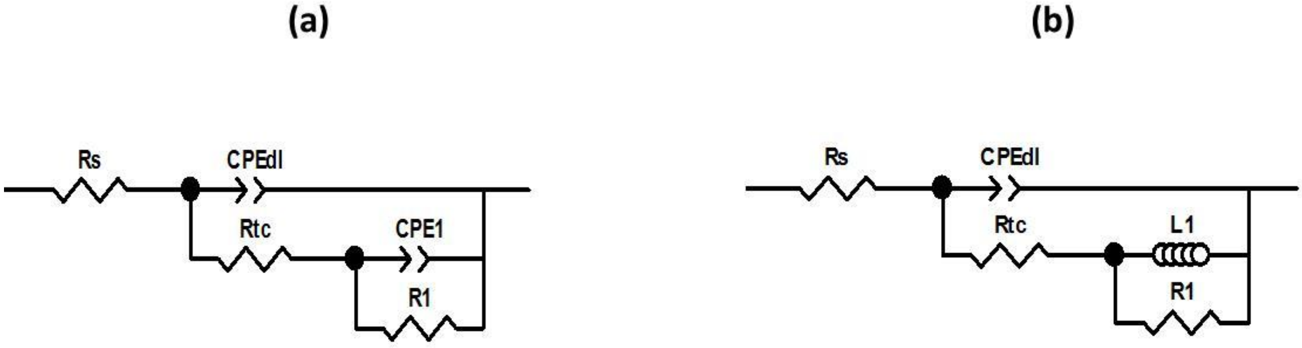

Figure 8. Equivalent electrical circuit used for the parameter regression calculation. a) For the electrolyte containing 400 g L^{-1} $Ni(NH_2SO_3)_2$, and for the electrolyte containing 400 g L^{-1} $Ni(NH_2SO_3)_2$ with 30 g L^{-1} H_3BO_3 at E = -1.1 V *vs.* Hg/HgSO$_4$. b) For the electrolyte containing 400 g L^{-1} $Ni(NH_2SO_3)_2$ with 30 g L^{-1} H_3BO_3 at E = -1.3 and -1.40 V *vs.* Hg/HgSO$_4$.

Table 3. EIS data of nickel electrodeposition onto Pt-QCM

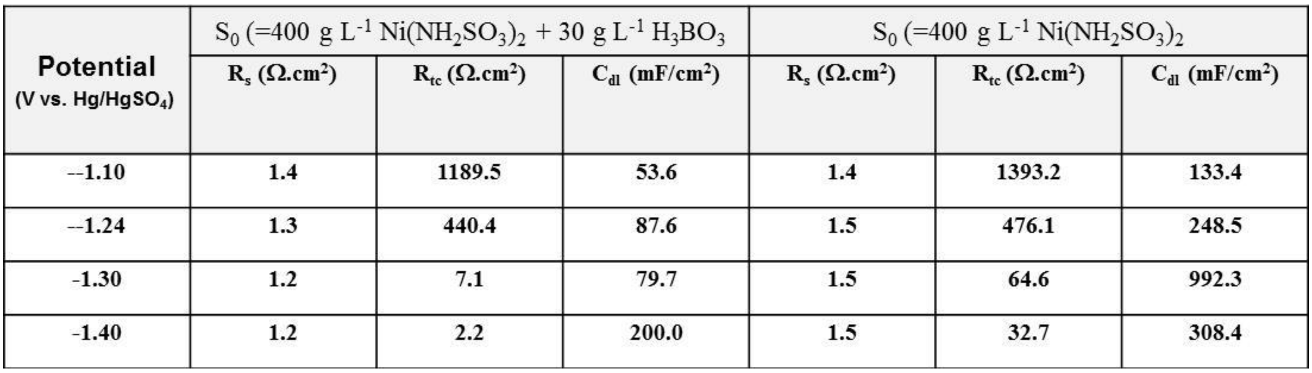

Potential (V vs. Hg/HgSO$_4$)	S_0 (=400 g L^{-1} $Ni(NH_2SO_3)_2$ + 30 g L^{-1} H_3BO_3			S_0 (=400 g L^{-1} $Ni(NH_2SO_3)_2$		
	R_s (Ω.cm^2)	R_{tc} (Ω.cm^2)	C_{dl} (mF/cm^2)	R_s (Ω.cm^2)	R_{tc} (Ω.cm^2)	C_{dl} (mF/cm^2)
--1.10	1.4	1189.5	53.6	1.4	1393.2	133.4
--1.24	1.3	440.4	87.6	1.5	476.1	248.5
-1.30	1.2	7.1	79.7	1.5	64.6	992.3
-1.40	1.2	2.2	200.0	1.5	32.7	308.4

Figure 9 presents AFM images obtained at different potential values ($E_{Deposition}$), corresponding to regions I, II and III of the voltammogram (Fig. 5). Fig. 9a corresponds to AFM image of the deposit obtained at $E_{Deposition}$ = -0.90 V for 15 min. The image shows that under these conditions the deposit formed is uniform but porous (due to the hydrogen evolution under these conditions). At $E_{Deposition}$ = -

1.30 V during the same time (Fig. 9b), the AFM image of the deposit reveals a compact coating composed of uniformly sized clusters. With the addition of boric acid, no holes were observed in the nickel coating at this potential. Under these conditions, the formation of bubbles associated with the hydrogen evolution reaction was minimized.

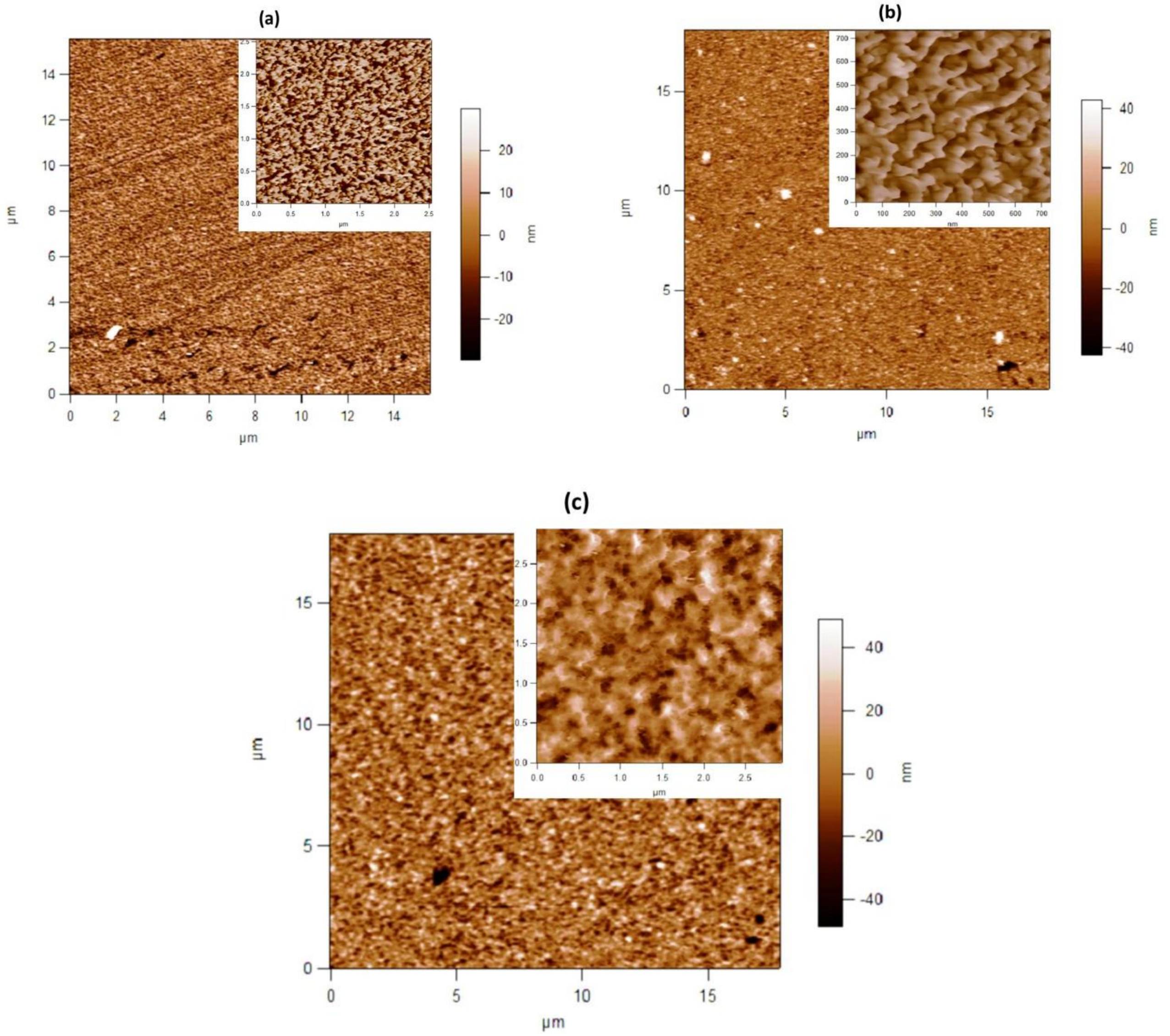

Figure 9. AFM images of nickel electrodeposition onto Pt-QCM electrode at: a) -0.90 V, b) -1.30 V and c) -1.40 V vs. $Hg/HgSO_4$. t = 15 min, Solution S_0 (=400 g L^{-1} $Ni(NH_2SO_3)_2$) with 30 g L^{-1} H_3BO_3.

Fig. 9c corresponds to the AFM image when the deposit was obtained at $E_{Deposition}$ = -1.4 V for 15 min. The image shows an amorphous deposit covering the substrate surface. On the basis of this result, we propose that in addition to the reduction of Ni, the insoluble species $Ni(OH)_{2(s)}$ is formed on the electrode surface at this potential region, due to the reduction of water (hydrogen evolution) and the resulting increase in local pH value in the vicinity of the working electrode. The AFM results corroborate those obtained by voltammetry and QCM.

4. CONCLUSIONS

The electrochemical deposition of nickel on Pt from a sulfamate bath, without and with boric acid was investigated using linear voltammetry, electrochemical impedance spectroscopy and Electrochemical Quartz Crystal Microbalance. The morphology of the deposited nickel was examined by atomic force microscopy. From the results obtained, the following conclusions can be made:

The analysis of the EQCM and EIS data during Ni electrodeposition from a sulfamate electrolyte without boric acid suggests the formation of a passivation layer ($Ni(OH)_{2(s)}$) with simultaneous Ni deposition in the potential range from -0.6 to -1.4 V vs. $Hg/HgSO_4$. The insoluble species $Ni(OH)_{2(s)}$ is formed on the electrode surface in this potential region, due to hydrogen evolution and the resulting increase in pH in the vicinity of the working electrode. The formation of nickel hydroxide in the absence of boric acid was confirmed by AFM.

In presence of boric acid in the solution, the analysis of the EQCM and EIS data during Ni electrodeposition in the potential range from -0.90 to -1.30 V suggests nickel deposition and reduction of boric acid. The AFM image of the deposit obtained at $E_{Deposition}$ = -1.30 V shows a compact coating made up of clusters with uniform size. With the addition of boric acid, no holes were observed in the nickel coating at this potential. Under these conditions the generation of bubbles associated with the hydrogen evolution reaction was minimized.

ACKNOWLEDGEMENTS
The authors are grateful for financial assistance provided by CONACyT, project CB 2009-01-128551. Celina E. Dávalos is grateful to CONACyT for scholarship support.

References

1. W.H. Remington, U.S. Patent 82,877 (1868).
2. I. Adams, U.S. Patent 93,157 (1869).
3. O.P. Watts, *Trans. Am. Electrochem. Soc.* 23 (1916) 395.
4. Jack W. Dini, Electrodeposition - The Materials Science of Coatings and Substrates, Noyes Publications, New Jersey (1993)
5. K.N. Njau, L.J.J. Janssen, *J. Appl. Electrocehm*. 25 (1995) 982.
6. A.M. Rashidi, A. Amadeh, *Surf. Coat. Technol.* 201 (2008) 3772-3776
7. W.G. Proud, E. Gomez, E. Sarret, E. Valles, C. Muller, *J. Appl. Electrochem*. 25 (1995) 770-775.
8. J. JI, W.C. Cooper, D.B. Dreisinger, E. Peters, *J. Appl. Electrochem*. 25 (1995) 642.
9. D. Grujicic, B. Pesic, *Electrochim. Acta* 51 (2006) 2678.
10. M. Holm, T.J. O´Keefe, *J. Appl. Electrochem*. 30 (2000) 1125.
11. D. Mockute, R. Butkiene, O. Nivinskiene, *Russian J. Electrochem*. 37 (2001) 376.
12. T. Mimani, S.M. Mayanna, N. Munichandraiah, *J. Appl. Electrochem*. 23 (1993) 339.
13. K.D. Song, K.B. Kim, S.H. Han, H.K. Lee, *Electrochem. Communications* 5 (2003) 460-466
14. M. Saitou and R. Hashiguchi, *J. Phys. Chem*. B 107 (2003) 9404.
15. M. Monev, M.E. Baumgartner, O. Leobich, Ch.I. Raub, *Metalloberflaeche* 45 (1991) 77.
16. F. Chassaing, M. Joussellin, R. Wiart, *J. Electroanal. Chem*. 119 (1981) 61.
17. F. Chassaing, M. Joussellin, R. Wiart, *J. Electroanal. Chem*. 157 (1983) 75.
18. R. Wiart, *Electrochim. Acta* 35 (1990) 1587.
19. R.D. Fisher, *J. Electrochem. Soc*., 109 (1962) 479., D. Baudrand, *Met. Finish*. 94 (1996) 15.

20. C. Karwas and T. Hepel, *J. Electrochem. Soc*., 135 (1988) 839.
21. A.A. EI-Shafei and A. Aramata, *J. Solid State Electrochem*. 11 (2007) 430.
22. A. Vicenzo and P.L. Cavallotti, *Russian J. of Electrochem*. 44 (2008) 716.
23. T. Mimani, S.M. Mayanna, N. Munichandraiah, *J. Appl. Electrochem*. 23 (1993) 339.
24. M. Supicová, R. Rozik, L. Trnková, R. Orinaková, M. Gálová, *J. Solid State Electrochem*. 10 (2006) 61.
25. R. Woods, in: A.J. Bard (Ed), *Electroanalytical Chemistry*, vol. 9, Marcel Dekker, New York, 1977, p.1.
26. G. Sauerbrey, *Z. Phys*. 155 (1959) 206.
27. K.K. Kanazawa and J.G. Gordon, *Anal. Chim. Acta* 175 (1985) 99.
28. M. Urbakh and L. Daikhin, *Langmuir* 10 (1994) 2836.
29. L. Daikhin, M. Urbakh, *Faraday Discuss*. 107 (1997) 27.
30. M. Yang, M. Thompson, W.C. Duncan-Hewih, *Langmuir* 9 (1993) 802.
31. G. Vatankhah, J. Lessard, G. Jerkiewicz, A. Zolfaghari, B.E. Conway, *Electrochim. Acta* 48 (2003) 1619.
32. H. Uchida, N. Ikeda, M. Watanabe, *J. Electroanal. Chem*. 424 (1997) 5.
33. H. Uchida, M. Hiei, M. Watanabe, *J. Electroanal. Chem*. 452 (1998) 97
34. M.C. Santos, D.W. Miwa, S.A.S. Machado, *Electrochem. Communicatios* 2 (2000) 692-696.
35. A.A. EI-Shafei *J. Electroanal. Chem*. 447 (1998) 81.
36. M. Keddam, J.F. Lizze, C. Pallota, H. Takenouti, *J. Electrochem. Soc*. 131 (1984) 2016.
37. Atlas of electrochemical equilibria in aqueous solutions, M. Pourbaix, Second Edition 1974, Ed. National Association of Corrosion Engineers, Houston Texas USA, 1974
38. A.P. Ordine, S.L. Díaz, I.C.P. Margarit, O.E. Barcia, O.R. Mattos, *Electrochim. Acta* 51 (2006) 1480.